ISSN 1061-3862, International Journal of Self-Propagating High-Temperature Synthesis, 2015, Vol. 24, No. 4, pp. 241–245. © Allerton Press, Inc., 2015.

Structural and IR study of $Ni_{0.5-x}Cd_xZn_{0.5}Fe_2O_4$

M. R. Patil[a], M. K. Rendale[b], S. N. Mathad[c], and R. B. Pujar[a, d]

[a] *S.S. Arts College & T.P. Science Institute, Sankeshwar, India*

[b] *Department of Engineering Physics, K.L.S. Gogte Institute of Technology, Belagavi, India*

[c] *Department of Engineering Physics, K.L.E. Institute of Technology, Hubli, India*

[d] *Department of Physics, P.C. Jabin Science College, Hubli, India*

e-mail: mkrendale@gmail.com; physicssiddu@gmail.com

Received July 15, 2015

Abstract—$Ni_{0.5-x}Cd_xZn_{0.5}Fe_2O_4$ ferrites ($x = 0.00$, 0.15, 0.30, and 0.45) have been synthesized by conventional ceramic method. The spinel phase purity and crystal lattice symmetry were estimated from X-ray diffraction studies. An infrared spectroscopy study shows the presence of main two absorption bands indicating the presence of tetrahedral and octahedral group complexes, respectively, within the spinel lattice. The main absorption bands of spinel ferrite were identified in the IR absorption spectra recorded in the range 300–700 cm^{-1}.

Keywords: Ni–Zn ferrites, Cd doping

DOI: 10.3103/S1061386215040081

1. INTRODUCTION

Ferrites are incomparable materials because of moderate magnetization, high permeability, reasonably high permittivity, and low losses at frequencies from dc to sub-millimeter wavelengths. These properties of ferrites suit them for high frequency applications [1]. Ferrites materials attained huge interest because of their unique magnetic, electric, and dielectric properties. They are extensively used in a wide range of applications from low to high permeability devices, including electronics, ferro-fluids, high density information storage devices, and magnetic drug delivery microwave devices [2–5]. Many works have been carried out on the substitution of cadmium (Cd) ion in spinel structure of ferrites [6, 7]. Ferrites have been studied and processed by versatile techniques such as co-precipitation method, aerosol method, modified oxidation process, hydrothermal process, and sucrose precursor sol–gel combustion forced hydrolysis ball-milling [5–10].

In this manuscript we report on the effect of cadmium doping on structural behavior of Ni–Zn ferrites ($Ni_{0.5-x}Cd_xZn_{0.5}Fe_2O_4$, $x = 0.00$, 0.15, 0.30, 0.45) synthesized by low-cost solid-state method. Doping with cadmium could be expected to change such parameters of ferrites as lattice constant, average grain size, strain, and IR spectra.

2. EXPERIMENTAL

Low-cost solid state ceramic method was used to prepare the ferrites with the general formula $Ni_{0.5-x}Cd_xZn_{0.5}Fe_2O_4$ ($x = 0.00$, 0.15, 0.30, and 0.45). High purity nickel oxide, cadmium oxide, zinc oxide and iron oxide were weighed accurately by using a microbalance in the required molar proportions and mixed mechanically in agate mortar in acetone medium. All samples were pre-sintered at 800°C for 10 h. Powders were subjected to hard milling in acetone medium and dried powders were sieved to obviate the large sized particles. Using hydraulic press (pressure of five tons for 5 min) pellets were prepared and subjected to final sintering at 1000°C by keeping them on alumina sheet in a silicon carbide furnace for 20 h to enable complete solid-state reaction. The flow chart of the process is shown in Fig. 1.

3. RESULTS AND DISCUSSION

3.1. XRD Analysis

X-ray diffraction has been used as a tool for structure determination (confirmation of spinel phase). According to Bragg's law, the diffraction maxima occur when

$$2d\sin\theta = n\lambda, \quad (1)$$

where n stands for the order of diffraction, λ is the X-ray wavelength, d interplanar distance, and θ glancing angle.

In case of cubic system, interplanar distance d is given by

$$d = a/(h^2 + k^2 + l^2)^{1/2}, \quad (2)$$

where a is a lattice parameter and (hkl) are Miller indices.

XRD patterns of $Ni_{0.5-x}Cd_xZn_{0.5}Fe_2O_4$ (see Fig. 2) are indexed in the light of the crystal structure of the natural spinel, $MgAl_2O_4$. According to it, the planes that diffract X-rays are (220), (311), (400), (422), (511), and (440). For the spinel ferrites the (311) peak is more intense. All the samples exhibit cubic spinel

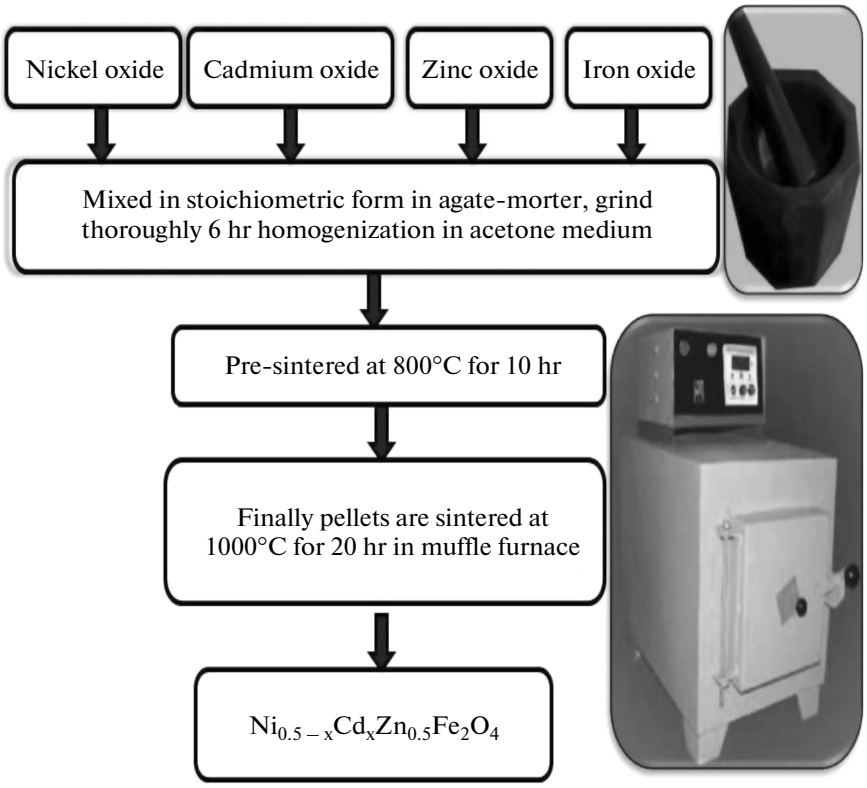

Fig. 1. Flow chart for synthesis of $Ni_{0.5-x}Cd_xZn_{0.5}Fe_2O_4$ ferrites.

structure. The absence of extra lines in the patterns confirms the formation of single phase ferrites. The prominent line in the diffraction pattern of spinels corresponds to the (311) plane. The observed and calculated values of interplanar distance d are collected in Table 1. There is a good agreement between the values of d_{obs} and d_{ctd}. The averaged grain size can be estimated by measuring a peak width at half maximum. The average crystallite size D for different x was calculated [11] by using the Debye–Scherrer formula:

$$D = \frac{0.9\lambda}{\beta \cos\theta}. \quad (3)$$

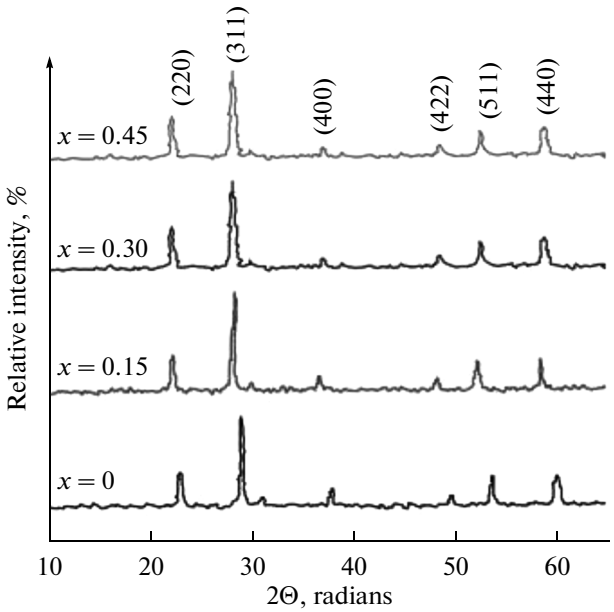

Fig. 2. XRD patterns of $Ni_{0.5-x}Cd_xZn_{0.5}Fe_2O_4$ ferrites.

The average crystallite size was found to be within the range 33–112 nm and to grow with increasing x. On the basis of ionic radii, the change in the lattice parameter is explained as follows: the radius of the Cd^{2+} ion (0.97 Å) is larger than that of the Ni^{2+} ion (0.69 Å). Changes in the cell parameter with increasing Cd^{2+} content may be attributed to a larger ionic radii of nickel, so that partial replacement leads to enlargement of the unit cell dimensions, and hence to changes in the lattice parameter [10–12]. The Cd^{+2} ions have larger ionic radius (0.97 Å) compared to those of Fe^{3+} (0.65 Å), Ni^{2+} (0.74 Å), and Zn^{2+} (0.74 Å) ions. The Cd^{2+} ions successively replace the Fe^{3+} ions on the A-site. Figure 3 presents lattice constant a as a function of Co content x. The variation in the lattice parameter indicates that the system under study conforms Vegard's law. Similar results have been obtained for Li–Ni [13] and Li–Cd ferrites [14–16]. Such a behavior can be described by using the 2-nd order polynomial

$$a = -0.998x^2 + 0.68x + 8.365 \quad (4)$$

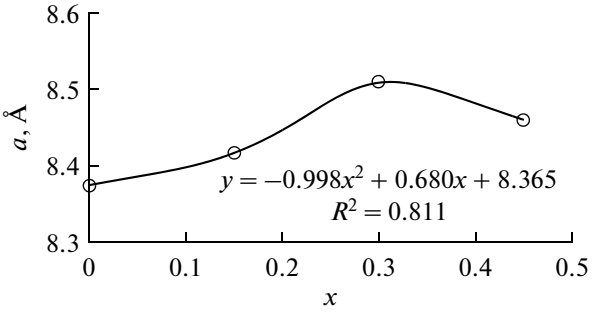

Fig. 3. Lattice constant a as a function of Co content x.

with regression coefficient $R^2 = 0.811$.

The number of dislocations in a unit volume of a crystalline material is expressed as dislocation density (ρ_D). Dislocations are one-dimensional crystalline defects marking the boundary between a slipped and an unslipped region of a material [10–12]. This defect distorts the regular atomic array of a perfect crystal. The amount of the defects in the as deposited film was resolved by evaluating the dislocation density [12]. Variations in micro strain ε and dislocation density ρ_D as a function of x were calculated from the expressions [10–12]

$$\rho_D = 1/D^2, \quad (5)$$

$$\varepsilon = \beta\cos\theta/4 \quad (6)$$

and the results are collected in Table 2.

3.2. Texture Analysis

Diffraction patterns from samples containing a random orientation of crystallites have predictable relative peak intensities. Texture in polycrystalline samples means some distinct spatial orientation of individual crystallites within the material [10–12]. The preferential crystal orientations were calculated from the texture coefficient (TC), defined as [12]

$$\mathrm{TC}(hkl) = \frac{\dfrac{I(hkl)}{I_0(hkl)}}{\dfrac{1}{N}\sum_N \dfrac{I(hkl)}{I_0(hkl)}}.$$

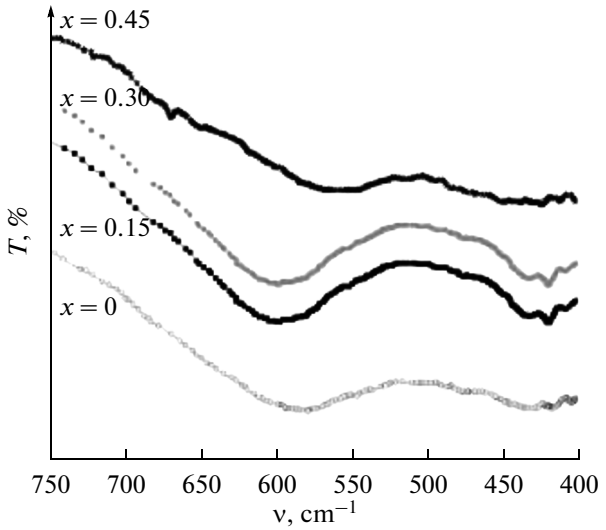

Fig. 4. FTIR spectra of $Ni_{0.5-x}Cd_xZn_{0.5}Fe_2O_4$ ferrites.

When 0 < TC (*hkl*) < 1, it is indicative of the lack of grains oriented in that direction. If TC (*hkl*) > 1, this means an abundance of grains with preferential orientation within the (400) plane. The preferred orientation of crystallite planes is characterized in Table 3.

3.3. FTIR Spectra

The spinel ferrites crystallize in the cubic spinel form with space group *Fd3m-O7h*. On the basis of group theoretical calculations, it has been shown that spinel ferrites exhibit four IR fundamentals in the vibrational spectra of normal and inverse spinel ferrites. It has been reported that first three IR bands are due to the tetrahedral (Td) and octahedral (Oh) coordination compounds, while the fourth one is due to some type of lattice vibrations involving tetrahedral cations [17]. Figure 4 shows the FTIR spectra of $Ni_{0.5-x}Cd_xZn_{0.5}Fe_2O_4$ ferrites. Positions of IR absorption bands along with their shoulders are tabulated in Table 4. The shoulders corresponding to principal bands I and II are designated as ν_{1s} and ν_{2s}, respectively.

Table 1. Miller indices (*hkl*) and lattice parameters (a)

	$x = 0.0$ ($a = 8.3747$ Å)		$x = 0.15$ ($a = 8.4157$ Å)		$x = 0.30$ ($a = 8.4600$ Å)		$x = 0.45$ ($a = 8.459$ Å)	
[*hkl*]	d_{obs}, Å	D_{ctd}, Å	d_{obs}, Å	D_{ctd}, Å	d_{obs}, Å	D_{ctd}, Å	d_{obs}, Å	D_{ctd}, Å
220	2.957	2.9592	2.9795	2.9795	2.9802	2.9815	2.9842	2.9863
311	2.5231	2.474	2.5422	2.5422	2.5633	2.5633	2.5751	2.5751
400	2.0931	2.0523	2.1082	2.1082	2.1212	2.1212	2.2102	2.2245
422	1.7094	1.6761	1.7007	1.7007	1.7331	1.7331	1.744	1.744
511	1.6131	1.5817	1.6226	1.6226	1.611	1.611	1.6447	1.6447
440	1.482	1.4531	1.4917	1.4917	1.4954	1.4922	1.4935	1.4946

Table 2. Parameters of $Ni_{0.5-x}Cd_xZn_{0.5}Fe_2O_4$ ferrites

x	D, nm	ε	$\rho_D \times 10^{15}$, m^{-2}
0.0	33	0.1195	90.084
0.15	44	0.1224	51.361
0.30	72	0.1273	19.316
0.45	112	0.1348	7.9847

Table 3. Texture coefficients for $Ni_{0.5-x}Cd_xZn_{0.5}Fe_2O_4$ ferrites

(*hkl*)	TC(*hkl*) $x = 0$	TC(*hkl*) $x = 0.15$	TC(*hkl*) $x = 0.30$	TC(*hkl*) $x = 0.45$
(220)	0.8540	0.9597	0.7155	0.7144
(311)	0.8271	0.9826	0.7524	0.7908
(400)	1.6145	0.8076	1.6786	1.2348
(422)	0.8924	1.0601	0.8118	0.8531
(511)	0.8365	1.0674	1.0031	1.1596
(440)	0.9788	1.1227	1.0388	1.2476

Table 4. Position of IR bands (cm^{-1}) for $Ni_{0.5-x}Cd_xZn_{0.5}Fe_2O_4$ ferrites

x	ν_1	ν_{1s}	ν_2	ν_{2s}	ν_3	ν_4
0.0	597	590	418	408	522	402
0.15	578	549	416	403	520	–
0.30	570	559	420	410	520	403
0.45	563	551	–	–	513	–

Waldon [18] studied IR spectra of spinel ferrites and attributed band ν_1 around 600 cm^{-1} to the intrinsic vibrations of tetrahedral complexes corresponding to the highest restoring force and band ν_2 around 400 cm^{-1}, to intrinsic vibrations of octahedral complexes. Therefore, it is expected that $\nu_1 > \nu_2$. Both ν_1 and ν_2 bands significantly depend on the nature of octahedral cations but not on the nature of octahedral ions [19]. Mössbauer and IR spectra of Ni–Zn ferrites suggest that the presence of Fe^{2+} ions on the octahedral site can lead to the splitting of IR absorption bands [20]. All our samples show (Fig. 4) two prominent absorption bands ν_1 and ν_2 at 550–600 cm^{-1} and 380–405 cm^{-1}, respectively, along with ν_3 band. The absorption becomes broader with an increase in x [21]. This was attributed to gradual transformation of long-range interaction to shorter-range one. A decrease in bands intensity was associated with a decrease in the ratio of Ni^{2+} to Fe^{3+} on B-site (down to 1 : 3) upon an increase in x [22]. In our case, the difference between positions of band ν_1 and band ν_2 is attributed to the difference in the Fe^{3+}–O^{2-} bond length in octahedral and tetrahedral coordination compounds [22].

The XRD data reveal that the lattice parameter increases linearly with increasing x. It is also known that an increase in the Fe^{3+}–O^{2-} bond length reduces the fundamental vibrational frequency. Therefore, the shift of the central frequency of all bands towards lower frequencies could be due to an increase in the lattice parameter caused by addition of cadmium [23]. Waldron [18] attributed bands ν_1 and ν_2 to the intrinsic vibrations of tetrahedral [Td] and octahedral [Oh] coordination compounds. Both these high-frequency bands have been attributed to the intrinsic lattice vibrations of E-symmetry. The third absorption band (ν_3) observed in some samples was attributed to the vibration of metal ions in the isotropic force field of their octahedral environment [18]. The splitting of the principal bands for the samples with $x = 0.00$–0.30 was associated with generation of the Jahn–Teller distribution by the non-cubic Fe^{2+} units that give rise to deformation of the cubic lattice. The decrease in intensity and complete disappearance of absorption bands for $x > 0.4$ suggests that the formation of Fe^{2+} ion is hampered by an increase in cadmium content, so that only the ν_1 and ν_2 bands still remain pronounced. Similar splitting and disappearance of IR absorption bands was reported in [22, 25].

3. CONCLUSIONS

In this paper, we have compared the behavior of lattice parameter (a), micro strain (ε) and texture coefficient (TC) for Cd^{2+}-substituted $Ni_{0.5-x}Cd_xZn_{0.5}Fe_2O_4$ ferrites upon variation in Cd content x. Remarkable changes in lattice parameter (from 8.3747 Å to 8.469 Å) with increasing x are due to a larger ionic radius of Cd^{2+}. The average crystallite size of the ferrite under consideration was found to vary within the range 33–112 nm. Texture analysis reveals adequate grain growth in different plane directions. The main absorption bands were recorded in the range 300–700 cm^{-1}. The splitting of the principal bands observed for the samples with $x = 0.00$–0.30 is attributed to the Jahn–Teller distribution generated by the non-cubic Fe^{2+} units that give rise to deformation of the cubic lattice.

REFERENCES

1. Harris, V.G., Advances in magnetics: Modern microwave ferrites, *IEEE Trans. Magn.*, 2012, vol. 48, no. 3, pp. 1075–1105.
2. Qu, Y., Yang, H., Yang, N., Fan, Y., Zhu, H., and Zou, G.T., The effect of reaction temperature on the particle size, structure, and magnetic properties of co-precipitated $CoFe_2O_4$ nanoparticles, *Mater. Lett.*, 2006, vol. 60, nos. 29–30, pp. 3548–3552.
3. Phillips, P.L., Knight, J.C., Mangan, B.J., Russell, P.St.J., Charlton, M.D.B., and Parker, G.J., Near-field optical microscopy of thin photonic crystal films, *J. Appl. Phys.*, 1999, vol. 85, no. 9, pp. 6338–6345.
4. Sousa, M.H. and Tourinho, F.A., New electric double layered magnetic fluids based on copper, nickel, and

zinc ferrite nanostructures, *J. Phys. Chem. B*, 2001, vol. 105, no. 6, pp. 1168–1175.
5. Iyer, R., Desai, R., and Upadhyay, R.V., Low temperature synthesis of nanosized $Mn_{1-x}Cd_xFe_2O_4$ ferrites, *Indian J. Pure Appl. Phys.*, 2009, vol. 47, pp. 180–185.
6. Sathishkumar, G., Venkataraju, C., and Sivakumar, K., Magnetic and dielectric properties of cadmium substituted nickel cobalt nanoferrites, *J. Mater. Sci: Mater. Electron*, 2013, vol. 24, no. 3, pp. 1057–1062.
7. Yattinahalli, S.S., Kapatkar, S.B., Ayachit, N.H., and Mathad, S.N., Synthesis and structural characterization of nano-sized nickel ferrite, *Int. J. Self-Propag. High-Temp. Synth.*, 2013, vol. 22, no. 3, pp. 147–150.
8. Singhal, S., Singh, J., Barthwal, S.K., and Chandra, K., Preparation and characterization of nano-size nickel-substituted cobalt ferrites (CoNiFeO), *J. Solid State Chem.*, 2005, vol. 178, no. 10, pp. 3183–3189.
9. Patil, N.D., Velhal, N.B., Tarwar, N.L., and Puri, V.R., Dielectric and magnetic properties of Co-substituted Ni–Cd ferrite prepared by solution combustion method, *Int. J. Eng. Innov. Technol.* (*IJEIT*) 2014, vol. 3, no 8, pp.73–77.
10. Rendale, M.K., Mathad, S.N., and Puri, V., Thick films of magnesium zinc ferrite with lithium substitution: Structural characteristics, *Int. J. Self-Propag. High-Temp. Synth.* 2015, vol. 24, no. 2, pp. 79–83.
11. Mathad, S.N. and Puri, V., Microwave studies of environmental friendly ferroelectrics, *Int. Schol. Res. Notices*, 2014, article ID 683986.
12. Mathad, S.N., Jadhav, R.N., Patil, N.D., and Puri, V., Structural and mechanical properties of Sr^{+2} doped bismuth manganite thick films, *Int. J. Self-Propag. High-Temp. Synth.*, 2013, vol. 22, no. 4, pp. 180–184.
13. Reddy, P.V. and Rao, T.S., Electrical conductivity of lithium-nickel ferrites, *Less-Common Met.*, 1981, vol. 79, no. 2, pp. 191–198.
14. Ravinder, D., Effect of sintering temperature on electrical conductivity of mixed lithium-cadmium ferrites, *Mater. Lett.*, 1999, vol. 40, no. 4, pp. 198–203.
15. Josyulu, O.S. and Sobhandari, J., DC Conductivity and dielectric behavior of cobalt–zinc ferrite, *Phys. Status Solidi A*, 1980, vol. 59, pp. 323–329.
16. Joshi, G.K, Deshpande, S.A., Khot, A.Y., and Savant, S.R., Microstructure and permeability studies of mixed Li–Cd ferrites, *Indian J. Pure Appl. Phys. A*, 1987, vol. 61 no. 3, pp. 251–258.
17. Kakatkar, S.V., Sankpal, A.M., Savant, S.R., Suryavanshi, S.S., Ghodake, U.R., and Kamat, R.K., Infrared absorption of Ti^{4+} and Zr^{4+} substituted Li–Zn ferrites, *Indian J. Pure Appl. Phys.*, 1994, vol.32, no. 2, pp. 193–194.
18. Waldron, R. D., Infrared spectra of ferrites, *Phys. Rev.*, 1953, vol. 99, no. 6, pp. 1727–1735.
19. Tarte, P. and Prudhomme, J., Infrared studies of spinels: I. A critical discussion of the actual interpretations, *Spectrochim. Acta*, 1971, vol. 27, no. 9, pp. 961–968.
20. Potakova, V.A., Zverev, N.D., and Romanov, V.P., On the cation distribution in $Ni_{1-x-y}Fe^{2+}_xZn_yFe^{3+}_2O_4$ spinel ferrites, *Phys. Status Solidi A*, 1972, vol. 12, no. 2, pp. 623–627.
21. Patil, S.A., Mahajan, V.C., Ghatage, A.K., and Lotke, S.D., Structure and magnetic properties of Cd and Ti/Si substituted cobalt ferrites, *Mater. Chem. Phys.*, 1998, vol. 57, no. 1, pp. 86–91.
22. Bellad, S.S., Pujar, R.B., and Chougule, B.K., Infrared studies of some mixed Li–Cd ferrites, *Indian J. Pure Appl. Phys.*, 1998, vol. 36, no. 10, pp. 598–601.
23. Patil, S.A., Otari, S.M., Mahajan, V.C., and Patil, A.B., Structural, IR, and magnetization studies on La^{3+} substituted copper ferrite, *Solid State Commun.*, 1991, vol. 78, no. 1, pp. 39–42.
24. Josyulu, O.S. and Sobhanadri, J., The far-infrared spectra of some mixed cobalt zinc and magnesium zinc ferrites, *Phys. Status Solidi A*, 1981, vol. 65, no. 2, pp. 479–483.
25. Reddy, P.V. and Reddy, V.D.J., Far-infrared spectral studies of some lithium-nickel mixed ferrites, *Magn. Magn. Mater.*, 1994, vol. 136, no. 3, pp. 279–283.